Author/s:
Pan, S;Richardson, JJ;Christofferson, AJ;Besford, QA;Zheng, T;Wood, BJ;Duan, X;Jara Fornerod, MJ;McConville, CF;Yarovsky, I;Guldin, S;Jiang, L;Caruso, F

Title:
Fluorinated Metal-Organic Coatings with Selective Wettability

Date:
2021-07-07

Citation:
Pan, S., Richardson, J. J., Christofferson, A. J., Besford, Q. A., Zheng, T., Wood, B. J., Duan, X., Jara Fornerod, M. J., McConville, C. F., Yarovsky, I., Guldin, S., Jiang, L. & Caruso, F. (2021). Fluorinated Metal-Organic Coatings with Selective Wettability. Journal of the American Chemical Society, 143 (26), pp.9972-9981. https://doi.org/10.1021/jacs.1c04396.

Fluorinated Metal–Organic Coatings with Selective Wettability

Shuaijun Pan,[1] Joseph J. Richardson,[1] Andrew J. Christofferson,[2] Quinn A. Besford,[1†] Tian Zheng,[3] Barry J. Wood,[4] Xiaofei Duan,[5] Maximiliano Jesus Jara Fornerod,[6] Christopher F. McConville,[7‡] Irene Yarovsky,[2] Stefan Guldin,[6] Lei Jiang,[8] and Frank Caruso*[1]

[1] ARC Centre of Excellence in Convergent Bio-Nano Science and Technology, and the Department of Chemical Engineering, The University of Melbourne, Parkville, Victoria 3010, Australia

[2] School of Engineering, RMIT University, GPO Box 2476, Melbourne, Victoria 3001, Australia

[3] Materials Characterisation and Fabrication Platform, and the Department of Chemical Engineering, The University of Melbourne, Parkville, Victoria 3010, Australia

[4] Centre for Microscopy & Microanalysis, The University of Queensland, Brisbane, Queensland 4072, Australia

[5] School of Chemistry, TrACEES Platform, The University of Melbourne, Parkville, Victoria 3010, Australia

[6] Department of Chemical Engineering, University College London, Torrington Place, London WC1E 7JE, UK

[7] School of Science, RMIT University, Melbourne, Victoria 3001, Australia

[8] CAS Key Laboratory of Bio-inspired Materials and Interfacial Sciences, Technical Institute of Physics and Chemistry, Chinese Academy of Sciences, Beijing 100190, China

*Corresponding author. E-mail: fcaruso@unimelb.edu.au

KEYWORDS: adherent coatings, decoupled wettability, heterogeneous chemistry, metal–organic coatings, superoleophobicity, superhydrophilicity

ABSTRACT: Surface chemistry is a major factor that determines the wettability of materials yet devising broadly applicable coating strategies that afford tunable and selective surface properties required for next-generation materials remains a challenge. Herein, we report fluorinated metal–organic coatings that concurrently display water-wetting and oil-repelling characteristics, a wetting phenomenon different from responsive wetting induced by external stimuli. We demonstrate this selective wettability with a library of metal–organic coatings using catechol-based coordination and silanization (both fluorinated and fluorine-free), enabling sensing through interfacial reconfigurations in both gaseous and liquid environments, and establish a correlation between the coating wettability and polarity of the liquids. This selective wetting performance is substrate-independent, spontaneous, durable, and reversible, and occurs over a range of polar and non-polar liquids (60 studied). These results provide insight into advanced liquid–solid interactions and a pathway toward tuning interfacial affinities and realizing robust, selective superwettability according to the surrounding conditions.

INTRODUCTION

Coating materials that display specific interfacial affinities have attracted extensive interest, especially in the fields of chemical production, adhesives, selective membranes, bio–nano interactions, and repellent materials.[1–6] The wettability of non-textured coatings is governed by surface chemistry,[6–8] and chemically homogeneous surfaces typically have defined wettability—either repellent or wetting for a given liquid. Lower surface tension liquids (e.g., oil) will wet better than higher surface tension liquids (e.g., water) for nearly all surfaces.[8–10] This phenomenon largely explains the challenge in creating surfaces with both water affinity and oil repellence properties.[10] Nevertheless, achieving simultaneous controlled surface affinity[11–15] and repellence to various liquids is important for engineering advanced materials[16] and holds promise and broad interest for a wide range of wetting-related applications such as self-cleaning, chemical sensing, and membrane separations.[17–32] Externally induced wetting, through e.g., shear and strain[33–35] or by combining surface active additives (e.g., chromophores),[36–43] can initiate responsive wettability.[44–48] However, externally induced wetting strategies do not lead to selective wetting without the application of specified external stimuli/energy or super-repellence to conventional wetting oils, in air or under water (e.g., droplet bouncing). Therefore, to date, a mechanistic understanding of selective wetting is largely unexplored. Furthermore, the development of broadly applicable coating strategies to achieve selective wettability remains a challenge.

Herein, selective and responsive wettability due to the surrounding fluid[49–51] are achieved through dynamic and reversible surface rearrangement of the nanocomposite coatings that integrate active motifs with diverse chemical affinities, i.e., covalent binding of a highly non-wetting material atop highly wetting metal–organic thin films

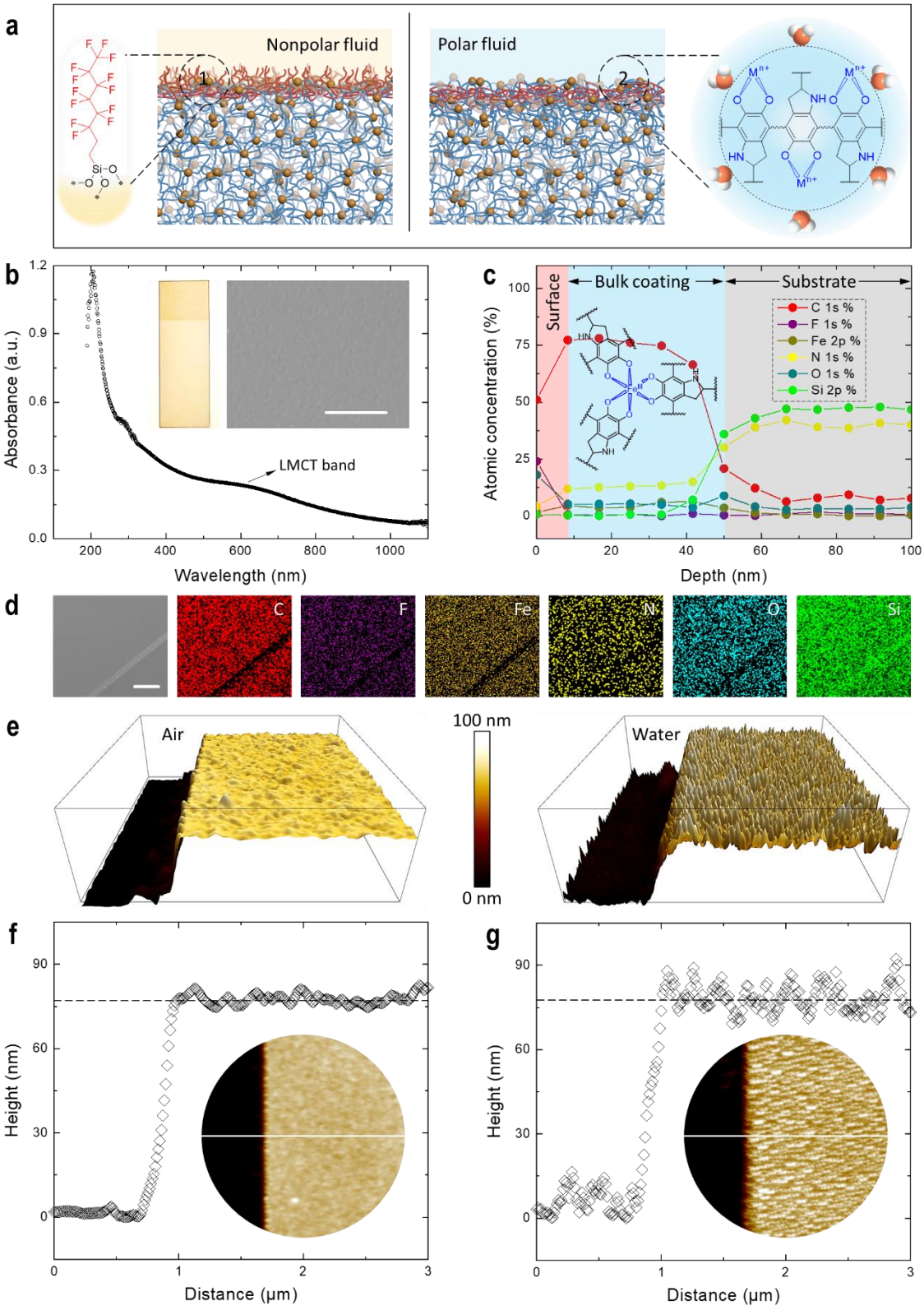

Figure 1. Design of repellent but polar heterogeneous nanocoatings. (a) Fluorinated metal–organic coatings (*f*MOCs) selectively respond to surrounding fluids according to their polarity and solvation ability, with a schematic of hydration (i.e., H_2O molecules) of the composite (M^{n+} represents metal ions) illustrated in the right panel. (b) UV–Vis spectra of *f*MOCs (fluorosilanized Fe^{III}–polydopamine coating). The insets show a photograph of the corresponding coated glass (2.6 × 7.6 cm^2) and associated scanning electron microscopy (SEM) image. Scale bar is 2 μm. (c) Chemical composition of *f*MOCs on a silicon nitride substrate, as determined by XPS. The inset illustrates a possible building block of the bulk coating. (d) EDS mapping of a scratched *f*MOC showing the elements present on the surface. Scale bar is 50 μm. (e) 3D AFM images of a *f*MOC (3 × 3 μm^2) in air and water. (f, g) Line profiles and 2D AFM images (insets) of a *f*MOC in air (f) and water (g). The black regions in (e–g) represent the scratched areas.

(Figure 1a). The nanocomposite coatings were engineered via the bio-inspired polymerization of metal–dopamine clusters[52] and subsequent surface modification (silanization) (Figures S1 and S2). We used two types of trialkyl silanes (i.e.,

1*H*,1*H*,2*H*,2*H*-perfluorooctyltriethoxysilane and its fluorine-free counterpart *n*-octyltriethoxysilane) as the precursors for surface silanization, as longer chain perfluorinated compounds (e.g., perfluorooctanoic acid or PFOA, perfluorooctanesulfonic acid or PFOS) are known to be toxic.[53–58] The metal–organic coatings (MOCs) examined have been selected because the dopamine component provides universal adherence and affinity to most common liquids (e.g., polar liquids), the metal–chelation networks are chemically stable, active and modular, and tunable repellence to various liquids is achieved through the integrated low energy silane component and the high energy MOC component which can respond (i.e., flip-flop[45,47] of the silane molecules) to the surrounding liquids based on their polarity (i.e., *f*MOCs; see *Materials and Methods* in the Supporting Information). Therefore, the resulting surface chemistry is heterogeneous, where both low surface energy silanes and high surface energy MOCs coexist in close proximity. In addition, the MOCs are intrinsically dynamic (or adaptive) owing to the nature of the coordination chemistry (between metal ions and the catechol moieties) exploited in the MOCs (i.e., reorganization of these components at the surface may occur).[59–61]

RESULTS AND DISCUSSION

The heterogeneous nature of *f*MOC chemistry was studied using conformal coatings assembled by Fe^{III}–dopamine clusters, evident from the ligand-to-metal charge transfer (LMCT) band at ~600 nm (Figure 1b). These coatings were transparent on diverse substrates (e.g., glass, silicon wafer, polytetrafluoroethylene, and polypropylene) and allowed for chemical modifications including the chemical deposition and condensation of silane molecules (Figure S3). The X-ray photoelectron spectroscopy (XPS) and depth profiling of a ~50 nm *f*MOC reveals the distribution of the active components (i.e., fluorine and MOCs) from the surface through to the silicon nitride substrate. The fluorine motifs are only detectable within the superficial layer (i.e., during the first etch, ~8 nm), while the coordination chemistry is identical throughout the MOC layer (i.e., ~3 organic ligands per metal center) (Figure 1c). Although all elements are present on the surface, as revealed by energy-dispersive X-ray spectroscopy (EDS) elemental mapping (Figure 1d), the ratio between the repellent and attractive motifs (i.e., F/O ratio) was, on average, two (Figure 1c). The abundance of O species on the *f*MOC surface (due to e.g., adsorption, oxidation, solvation and/or preservation from MOC; Figures S4 and S5) coexisting at a comparable coverage (~30 at.%) with fluorine species that are present as a thin surface layer (<10 nm; Figure 1c) not only suggest the heterogeneous chemistry nature of *f*MOC, but also when combined with the amorphous nature of the coating could allow dynamic interfacial rearrangement and polar interactions with the MOCs.

In liquid, surface reconfiguration of *f*MOC, confirmed by atomic force microscopy (AFM), was more discernible when compared with that in air (Figure 1e). The root-mean-square (RMS) roughness of the *f*MOCs following immersion in water (~4 nm) was more than twice as large as that of the dry *f*MOCs (~1.5 nm). This change is unlikely due to solvent swelling of the *f*MOCs (as the mean thickness of the film remained unchanged) but more likely due to the reconfiguration of the film occurring at the chemically heterogeneous surface (Figure 1f and 1g). This reconfiguration not only provides a blueprint for engineering selective wetting but also expands the toolbox of reconfigurable materials.

Surface Interactions and Wettability. Lateral force microscopy (LFM) investigations offered insight into the structural basis of reconfigurations observed in *f*MOCs (Figure 2a), provided their surface roughness was largely <1 nm in air (i.e., microscopically smooth, thereby enabling the study of the intrinsic interfacial frictions with given probes). As the LFM probes were rendered hydrophilic upon treatment with UV–O_3 for 10 min, higher signals in LFM images represent stronger hydrophilic interactions.[62] Hydrophilic (blue) domains with irregular nano-shapes that coexisted with the repellent (red) regions for *f*MOCs (Figure 2a) were largely preserved from the bulk MOCs (Figures S6 and S7), facilitating the selective and dynamic response of *f*MOC surfaces to water. Notably, conventional repellent surfaces (e.g., fluorosilanized silicon wafer, *f*Silicon; Figure 2b) displayed negligible differences, confirming their homogeneous repellence nature (similar to Teflon), which is also evident from the color clustering analysis of the LFM images (Figures S7 and S8). The LFM experiments show that the *f*MOC is intrinsically polar despite being modified by non-polar silane molecules. Surface adhesion force measurements were also performed to demonstrate the difference between a conventional fluorinated surface (*f*Silicon) and *f*MOCs (Figure 2c). The *f*MOCs featured a snap-off force with the hydrophilic probe when retracting the probe from the surface in contrast to the repulsive force profile observed for *f*Silicon. It is noted that this non-conventional surface behavior was also observed for an alkanesilane-modified MOC surface (*a*MOC) (Figure S9), highlighting the generalization of the proposed design principle and its potential for engineering fluorine-free (thereby environmentally friendly) surfaces with selective wettability, although fluorocarbons have been reported as suitable platforms/interface materials for studying biosystems.[63] These LFM results and atomic adhesion force measurements not only highlight the static interfaces of *f*Silicon (i.e., non-responsive) compared with the adherent and responsive interfaces of *f*MOC (Figures S6–S9), but also emphasize the synergistic interplay and roles of the different species for the selective wettability of *f*MOCs.

The selective wetting of these *f*MOCs was also examined through the spreading dynamics of droplets (i.e., water, *n*-hexadecane) (Figure 2d). Oil droplets displayed virtually no spreading (contact angle ~75°), as predicted assuming homogenous surface chemistry (Movies S1 and S2). In contrast, the water droplet spread quickly (<1 s) until equilibrium (~23°), which is contrary (or counterintuitive) to what is expected for a typical repellent surface (*f*Silicon) (Movies S3 and S4). This observation is likely due to the interfacial reconfiguration of the *f*MOCs or the possible conformation/distribution changes of the surface additives.[64] Surface energy analysis provides a mechanistic

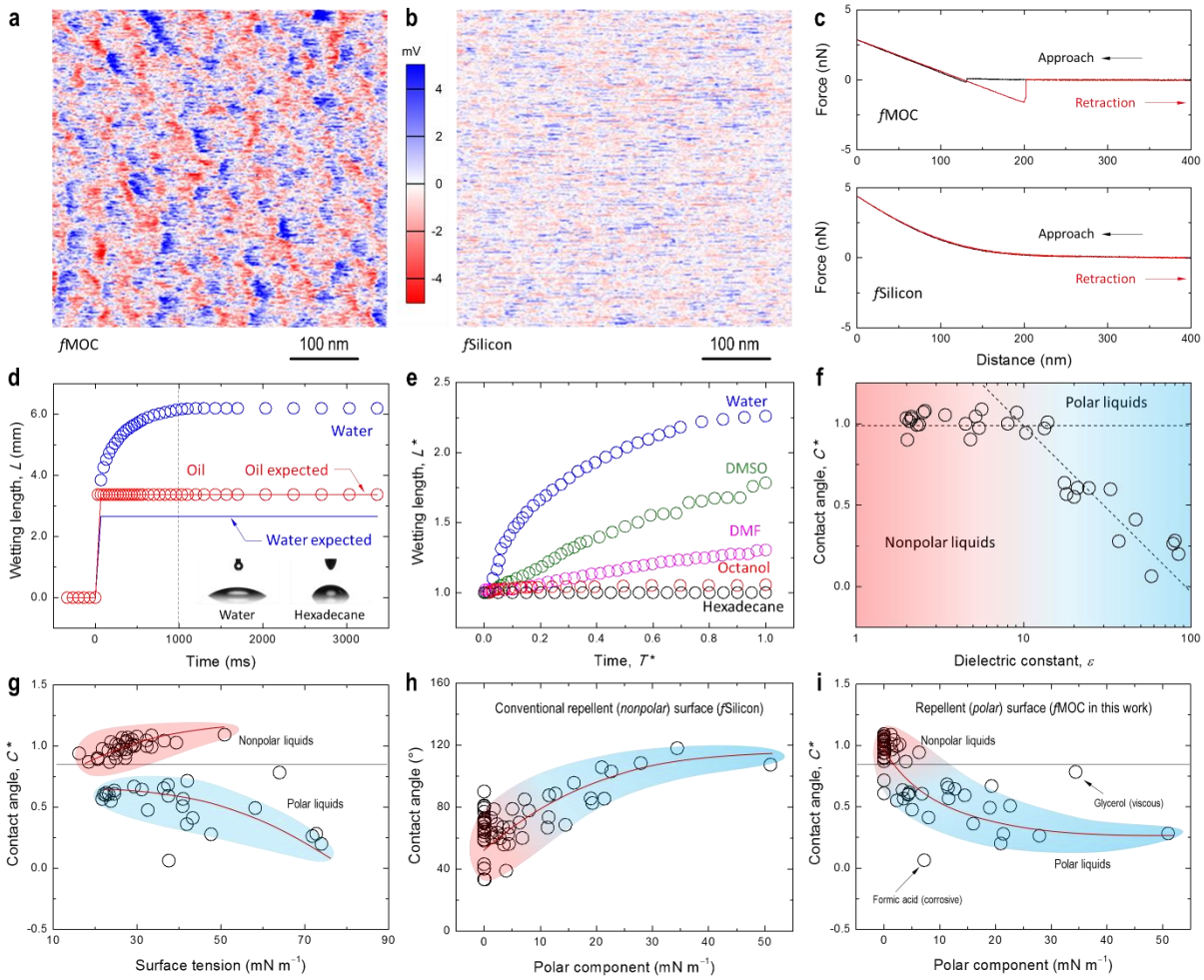

Figure 2. Selective water affinity and oil repellence. (a) LFM image of *f*MOC (0.5 × 0.5 μm^2), showing microscopically hydrophobic (red) and hydrophilic (blue) domains. (b) LFM image of *f*Silicon control (0.5 × 0.5 μm^2). (c) Representative atomic adhesion force curves of *f*MOC and *f*Silicon determined by colloidal-probe AFM. (d) Dynamics of the wetting length (diameter of the triple-phase contact line) of ~5 μL liquids. Data of *f*Silicon are presented by the (expected) lines. The insets are the silhouettes of water (left) and oil (right) droplets. (e) Wetting length (normalized with the droplet initial diameter) against the wetting time (normalized with the maximal wetting time). (f) Contact angle (normalized by conventional repellent control *f*Silicon) as a function of dielectric constant of the liquids. See Table S1 for liquids information. (g) Normalized contact angle of *f*MOC as a function of surface tension of the liquids studied. (h, i) Contact angle of *f*Silicon (h) and normalized contact angle of *f*MOC (i) as a function of polar component of the liquids studied. The red lines and shaded areas (g–i) are visual guidelines. The black lines (g and i) serve as an indicative boundary between polar and non-polar liquids, in contrast to their non-selective control (h). Indicated outliers are due to their corrosive nature or viscous dissipation.

understanding of the selective wettability, showing the interplay of surface wetting and non-wetting forces. The *f*MOCs have substantially different surface energy components (i.e., heterogeneity), namely a surface repellent non-polar component (fluorine) and a hydrophilic polar component (MOC), in contrast to less polar (lower energy) materials such as Teflon, polypropylene, and polydimethylsiloxane. Another characteristic of the *f*MOCs is the presence of repellent motifs (i.e., fluorosilane) on top of the hydrophilic and dynamic MOC, and a reasonably low degree (e.g., F/O atomic ratio ~2) of non-polar surface chemistry affords selective and responsive wettability determined by the interplay of interfacial energies.

Further experiments indicated that the selective wetting also occurred for a diverse range of liquids (including *n*-hexadecane, *n*-octanol, dimethylformamide, dimethyl sulfoxide, and water), with water and oil, respectively, resulting in the most and least wetting properties (Figure 2e) regardless of the nature of the substrate. The selective wetting phenomenon also applied to a series of *f*MOCs containing different metal ions[65] with nanoscale thickness (20–100 nm), tunable roughness and wettability, as well as transient timescale of reconfiguration (e.g., time of spreading is tunable and mostly ~0.2 s). The selective and spontaneous wetting of polar liquids also provides insights into the heterogeneous surface regime of *f*MOCs (i.e., high polar interactions) and its potential in liquid separation afforded by its non-wetting property to non-polar liquids (which are typically preferentially wettable owing to their low surface tensions). In addition, the different binding constants[66] between a given organic ligand (catechol) and different metal ions are expected to allow tuning of the stability of heterogeneous *f*MOCs.

To further examine the surface wettability, 32 liquids with different physiochemical properties (i.e., ε values ranging from 2 to 100) were examined (Figure 2f, Table S1). Liquid (as-placed or static) contact angles[67,68] on

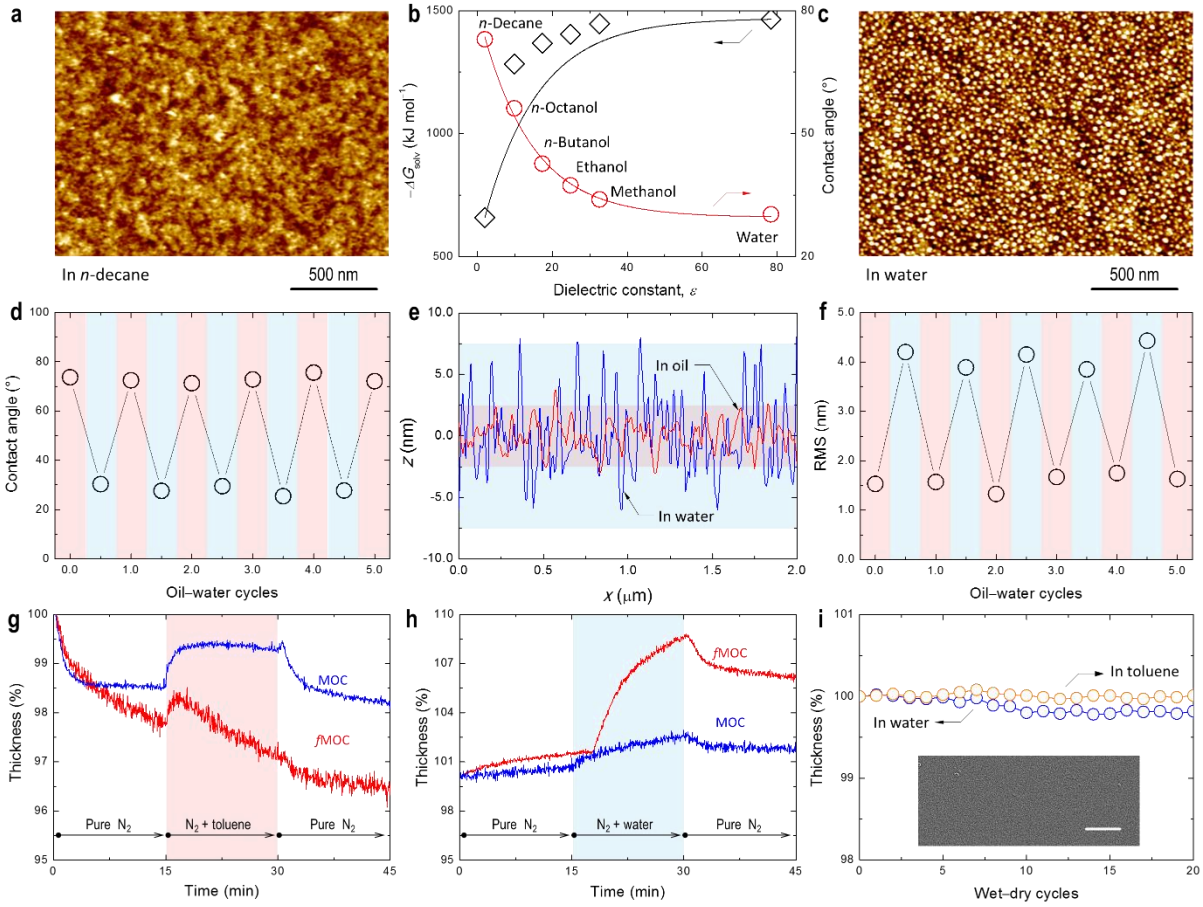

Figure 3. Reversible topology and wettability. (a) AFM image of *f*MOC in oil (*n*-decane). Scale bar is 500 nm. (b) Correlation between calculated solvation energy (diamond) of Fe^{III}–dopamine clusters and the experimental *f*MOC surface wettability (circle). (c) AFM image of the coating (a) in water. Scale bar is 500 nm. (d) Contact angles of oil (*n*-hexadecane) and water as a function of cycle number. The cyclic test involved successive contact measurements using a new droplet for each new cycle after removing the old droplet by blowing nitrogen. (e) Representative AFM line profiles of the *f*MOC in *n*-decane and water. (f) RMS roughness of the *f*MOC as a function of cycle number (in *n*-decane and water). (g, h) Thickness variation of MOC and *f*MOC thin films exposed to a (g) toluene atmosphere and (h) water atmosphere. (i) Durability of *f*MOC over 20 wet–dry cycles (either bulk oil or water was used to wet the coating via immersion for 5 min, followed by drying in nitrogen). The inset shows a helium ion microscopy image of the undamaged *f*MOC film even after 20 wet–dry cycles. Scale bar is 1 μm.

*f*MOCs were normalized by their controls, excluding interfacial liquid confinement.[69] The surface was passive to all of the non-polar liquids studied but displayed selective affinity to the polar liquids, which can be also seen from the increased contact angle hysteresis of polar liquids, in contrast to the conventional repellent and non-polar surfaces (e.g., *f*Silicon) (Figure S10). To provide further insights into surface regimes, the wettability of 60 liquids (see *Probe Liquids* in *Materials and Methods* in Supporting Information) was plotted against their surface tension (consisting of polar (p) and non-polar (dispersive; d) components, i.e., γ_l^p and γ_l^d, respectively) (Figure 2g–2i). *C** is a measure of the extent that *f*MOC differs from the *f*Silicon control, i.e., conventional repellent (non-polar) surface. *C** ~1 indicates that *f*MOC has a comparable surface property with *f*Silicon control, whereas *C** ~0 indicates a complete reversed interfacial property, i.e., non-conventional repellent surface with preserved selective affinity. Contrary to the observation made for the conventional repellent surfaces (i.e., non-polar *f*Silicon, Figure 2h), the contact angles of the liquids residing on our polar *f*MOC clustered in two regions (Figure 2g) and, in general, coincided with the surface tension of their predominant polar components (Figure 2i). For example, *f*Silicon follows the Young's equilibrium[67,68] at the triple phase contact line of a droplet at the surface, i.e., $\cos\theta \sim (\gamma_l^p + \gamma_l^d)^{-1}$ for a given surface energy (Figure 2h). This principle applies for conventional surfaces but does not apply for the heterogeneous *f*MOCs that attract polar liquids strongly, as indicated by the two separate regions observed in Figure 2g. As for *f*MOCs, the relation between liquid contact angle and its surface tension components has to be considered separately as $\cos\theta \sim (\gamma_l^d)^{-1}$ for non-polar liquids and $\cos\theta \sim (\gamma_l^p)^{-1}$ for polar liquids. This decoupled relation together with *C** thereby allow prediction of surface wettability of heterogeneous surfaces and their degree of surface heterogeneity. This finding is consistent with other correlations determined from parameters used to evaluate liquid polarity including dipole moment,[70] permittivity,[71] polarity index,[72] and empirical parameters[73] (Figure S11), thereby demonstrating the heterogeneous nature of *f*MOC. It is noted that the selective wettability may also be partially ascribed to the zeta potential of *f*MOC (tunable within the range of −60 to 60 mV at pH 1–12; Figure S12) and/or the ionic strength[74,75] but is not related to surfactant-driven

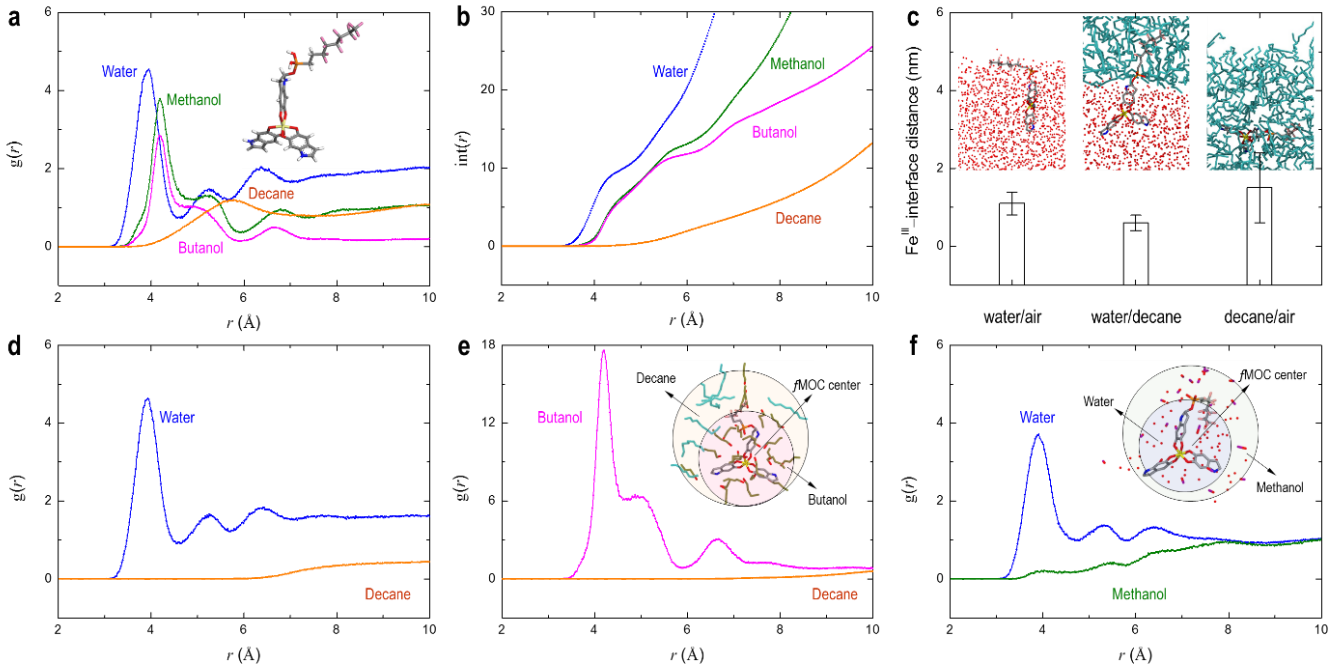

Figure 4. Molecular dynamics simulations of solvation shell and solvation selectivity of *f*MOC with liquids. (a, b) Radial distribution functions g(*r*) (a) and integrals int(*r*) (b) between Fe^{III} *f*MOC (inset) and different liquids (from polar to non-polar: water, methanol, butanol, and decane). (c) Distance from center of *f*MOC (e.g., Fe^{III}) to the interface and representative snapshots from MD simulations of the model *f*MOC subunit in water, 1:1 (v/v) water/*n*-decane (immiscible) mixture, and *n*-decane with a solvent–air interface. Five independent simulations for each system were generated and error bars are standard deviations. (d–f) Radial distribution functions g(*r*) between Fe^{III} *f*MOC and oxygen (or carbon for decane) in three liquid mixtures (1:1 v/v): immiscible water/*n*-decane mixture (d), miscible organic (*n*-butanol/*n*-decane) mixture (e), and miscible aqueous (water/methanol) mixture (f). The insets show the corresponding solvation shell states.

transient wetting based on the unchanged liquid surface tensions before and after contacting the *f*MOCs (Table S2). This unaltered liquid property also indicates that *f*MOCs are chemically stable when contacting the probing liquids—a prerequisite for durable interface reversibility.

Interface Reversibility. In addition, alcohol homologs were chosen (i.e., *n*-octanol, *n*-butanol, ethanol, and methanol) to evaluate the potential solvation effects and morphology changes when exposed to different liquids (Figure 3a–3c). Previous studies[49–51] have shown that some functional groups are more exposed to the surface than others as a function of the liquid above the solid. Our results also showed that the selective wetting is inversely correlated to the solvation energies of the Fe^{III}–dopamine clusters (i.e., the solvation free energy, ΔG_{solv} (see *Quantum Mechanics (QM) Calculations of Solvation Free Energy* in the Supporting Information), decreases with increase in contact angle) (Figure 3b). Importantly, the selective wetting was reversible, and no obvious change was observed after 100 measurement cycles (where one cycle refers to one iteration of exposure to oil and water, data of 5 cycles of measurements are shown in Figure 3d). This was apparent from the nanoscale surface configurations (e.g., height profile) of *f*MOCs in the corresponding liquids (Figure 3e), where control unmodified coatings showed negligible reconfiguration (Figure S13). In addition, we investigated the nanoscale surface reconfiguration and reversibility by measuring the surface roughness of the coatings when subjected to multiple oil–water immersion cycles (observing changes within a single cycle only was not feasible as these changes occurred within a short timescale of ~1 s). The surface roughness was largely preserved over multiple cycles of AFM measurements (e.g., RMS in Figure 3f), with negligible changes over 100 repeated tests (i.e., intrinsically dynamic nature) (Figure S14). It is noted that the extent of surface reconfiguration is typically in line with the polarity of the surrounding liquids (Figure S15) and can be further altered by the incorporation of different metal ions. The selective wetting behavior of the *f*MOCs to surrounding environments also applies to gaseous conditions. Specifically, the thickness of the *f*MOCs was monitored in real time by ellipsometry during their exposure to dry nitrogen and solvent vapors (i.e., toluene, water) (Figure 3g and 3h). The variations in thickness revealed the specific interaction between the surface and the vapor. For example, the decrease in thickness observed in Figure 3g indicated the desorption of moisture from the *f*MOC surface when non-polar toluene vapor was introduced, whereas the increase thickness in Figure 3h indicated the reconfiguration of *f*MOC due to the surrounding water vapor. The results highlight that the *f*MOCs are sensitive to water vapor (polar) but relatively inert to gas-phase toluene (non-polar). That is, the coating displays composition-dependent selective response to the gaseous environment. In contrast, the unmodified MOCs had negligible selectivity, which explains the importance of surface heterogeneity, which is present in *f*MOCs, for selective wetting. Notably, *f*MOCs are stable over 20 wet–dry cycles (Figure 3i) and after long-term (up to 10 days tested) immersion tests in water and oil (determined from the negligible changes observed in coating thickness, zeta potential, and refractive index), reversible morphology tests (Figure 3f, Figure S14), and liquid surface tension tests (Table S2).

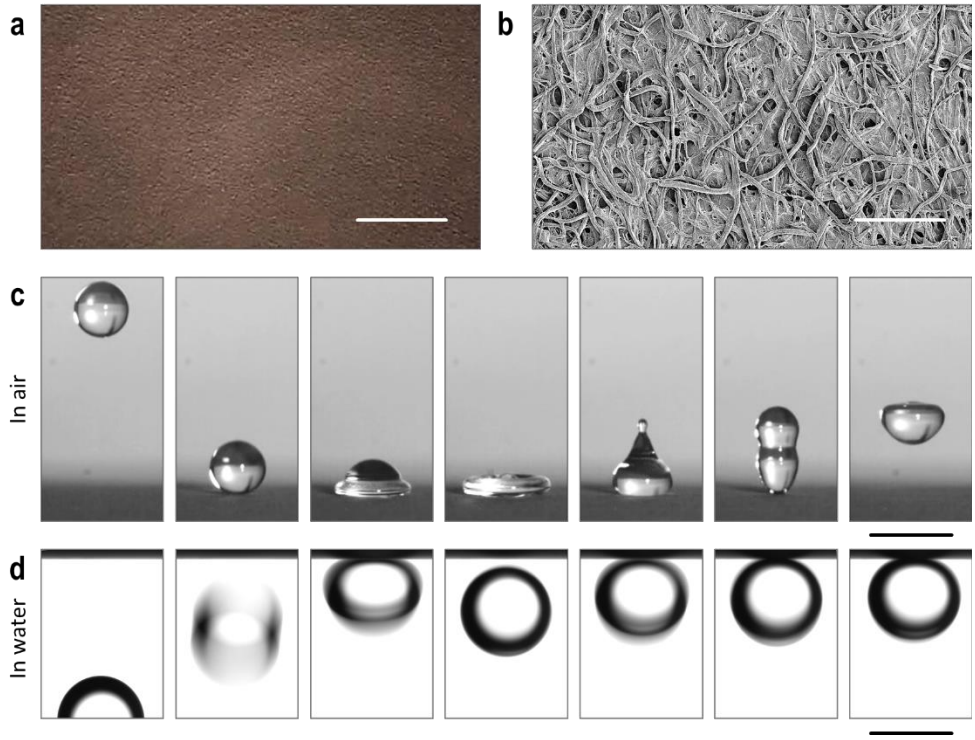

Figure 5. Robust super-repellence to oil in either air or water. (a, b) Digital and SEM images of a coarse substrate (filter paper) after *f*MOCs treatment. Scale bars are 1 cm and 500 μm, respectively. (c, d) Bouncing oil droplets (*n*-hexadecane) on the coated substrate either placed in air (c) or immersed in water (d). Scale bars are 5 mm. Time intervals are ~4 and ~10 ms, respectively.

Molecular Mechanistic Study. Molecular dynamics (MD) simulations were performed (see *Materials and Methods* in the Supporting Information) to obtain a further understanding of the interfacial interactions of the heterogeneous chemistry of *f*MOC and its selective wettability (Figure 4, Figure S16). By placing the subunit of *f*MOC coating (i.e., *f*MOC cluster) in different liquids with varying polarities, solvation can be represented by the radial distribution function peak maximum (i.e., solvation shell; Figure 4a) and the integrals (Figure 4b). It is noted that the subunit of *f*MOC simulated as an all-atom film simulation was not feasible but should provide a basic understanding of the heterogenous *f*MOC structure. Molecules of polar liquids (e.g., water, alcohols) associate with *f*MOC within closer proximity when compared with non-polar liquid (e.g., *n*-decane) (Table S3), indicating the higher affinity of *f*MOC to polar liquids than non-polar liquids. In addition, the molecular mechanistic of the selective wettability of *f*MOC can be evaluated by MD simulations using liquids mixtures either immiscible or miscible (Figure 4c–4f). The *f*MOC–solvent interactions can be explained by their selective occurrence at the phase interface with the polar motif residing on the polar phase (Figure 4c) and the selective solvation in mixed (competitive) environments including immiscible water/decane mixture (Figure 4d), miscible and less polar butanol/decane system (Figure 4e), and miscible and polar water/methanol system (Figure 4f). These MD simulations collectively support the selective water-wetting–oil-hating behavior of the heterogeneous *f*MOCs.

Superwettability. The non-conventional wetting regime was further applied to and could be further enhanced by coarser substrates (Figure 5a and 5b). The selective wetting was examined in both air and liquid. For example, an oil droplet bounced off an *f*MOCs-coated filter paper both in air (Figure 5c) and water (Figure 5d) without penetration, demonstrating super-repellence to oil (Movies S5 and S6). The super-repellence achieved (i.e., contact angle >150°, roll-off angle <10°, and droplet bouncing both in air and in liquid) can be ascribed to the reduced solid–liquid contact on coarser substrate (i.e., higher degree of structural hierarchy tiers)[6] and also indicate the potential for tuning surface selective repellence and affinity. Furthermore, these surfaces displayed selective super-affinity to a polar liquid (e.g., water) in both air and oil environments (Figure S17, Movies S7 and S8). Collectively, these findings demonstrate extreme instances of selective wetting and highlight how heterogenous coatings can open new routes to studying fundamental questions in surface wettability.

CONCLUSION

A coating strategy for engineering selective surface wettability is developed by combing metal–organic chemistry and low-energy silanization. Both experimental and computational results reveal that the *f*MOCs are heterogeneous in nature and display an unexpected wetting mechanism: the coexistence of repellence to low surface tension oils and wetting by polar and/or high surface tension liquids such as water. Unlike conventional repellent surfaces where the degree of surface repellence (i.e., from high to low) follows the order of liquid surface tension (i.e., from high to low), the present heterogeneous *f*MOC surfaces display repellence/wetting that follows the order of both liquid surface tension and their polarity. The heterogeneous *f*MOCs are capable of decoupling the interfacial polar and nonpolar interactions with quantitative correlations determined, providing a general pathway that allows for advanced and selective wettability engineering, e.g., the coexistence and decoupled oil repellence and liquid wetting (for polar liquids) enables gravity-driven (highly energy efficient) liquid separations. Although further experiments are required for a complete understanding of the interplay between materials and fluids,[18,67,76,77] the flexibility of designing tunable interfaces contributes to the knowledge of

nature-inspired superwetting systems.[20] This highlights that the engineering of coatings with selective wettability is not only feasible but also promising for on-demand practical applications in a wide range of fields, e.g., selective liquid sieving, fog harvesting, oil spill clean-up and recycling, and environment-friendly cleaning of clothes and surfaces.

ASSOCIATED CONTENT

Supporting Information. Materials and methods (coating preparation, vapor sensing, surface adhesion, lateral force analysis, wettability and selectivity studies, quantum mechanics calculations, MD simulations, and characterization), Figures S1–S17 (surface chemistry, lateral force imaging, fluorine-free coatings, contact angle hysteresis, correlation between wettability and polarity, AFM roughness and responsiveness, MD simulations, and decoupled superhydrophilicity), Tables S1–S3 (properties of probing liquids and solvation data), and Movies S1–S8 (selective wetting/nonwetting and superwettability of coatings in air and in liquid). This material is available free of charge via the Internet at http://pubs.acs.org.

AUTHOR INFORMATION

Corresponding Author

* fcaruso@unimelb.edu.au

Present Addresses

† Leibniz-Institut für Polymerforschung e.V., Hohe Str. 6, 01069 Dresden, Germany.

ǂ Institute for Frontier Materials, Deakin University, Geelong, Victoria 3216, Australia.

Funding Sources

This research was conducted and funded by the Australian Research Council Centre of Excellence in Convergent Bio-Nano Science and Technology (F.C., Project No. CE140100036). F.C. acknowledges the award of a National Health and Medical Research Council Senior Principal Research Fellowship (GNT1135806). This research was also supported by the National Natural Science Foundation of China (S.P., Grant No. 51703056), Natural Science Foundation of Hunan Province of China (S.P., Project No. 2018JJ3028), and Pawsey Supercomputing Centre and the National Computational Infrastructure of Australia (I.Y., Grant Nos. e87 and LE170100200).

Notes

The authors declare no conflict of interest. All authors have given approval to the final version of the manuscript.

ACKNOWLEDGMENT

We thank Q.-Z. Zhong, J. Zhou, R. Guo, B. Noble, T. Bai, W. Xu, and J. Jiang for helpful discussions and/or support with the characterization studies.

ABBREVIATIONS

MOC, metal–organic coating; *f*MOC, fluorinated metal–organic coating; *a*MOC, alkanesilane-modified MOC; *f*Silicon, fluorosilanized silicon wafer; SEM, scanning electron microscopy; XPS, X-ray photoelectron spectroscopy; LMCT, ligand-to-metal charge transfer; EDS, energy-dispersive X-ray spectroscopy; LFM, lateral force microscopy; AFM, atomic force microscopy; RMS, root-mean-square; MD, molecular dynamics.

REFERENCES

(1) Guo, J.; Suástegui, M.; Sakimoto, K. K.; Moody, V. M.; Xiao, G.; Nocera, D. G.; Joshi, N. S. Light-driven fine chemical production in yeast biohybrids. *Science* **2018**, *362*, 813–816.

(2) Li, J.-J.; Zhou, Y.-N.; Luo, Z.-H. Polymeric materials with switchable superwettability for controllable oil/water separation: A comprehensive review. *Prog. Polym. Sci.* **2018**, *87*, 1–33.

(3) Lee, H.; Lee, B. P.; Messersmith, P. B. A reversible wet/dry adhesive inspired by mussels and geckos. *Nature* **2007**, *448*, 338–341.

(4) Cobo, I.; Li, M.; Sumerlin, B. S.; Perrier, S. Smart hybrid materials by conjugation of responsive polymers to biomacromolecules. *Nat. Mater.* **2015**, *14*, 143–159.

(5) Kim, Y.; Macfarlane, R. J.; Jones, M. R.; Mirkin, C. A. Transmutable nanoparticles with reconfigurable surface ligands. *Science* **2016**, *351*, 579–582.

(6) Pan, S.; Guo, R.; Bjornmalm, M.; Richardson, J. J.; Li, L.; Peng, C.; Bertleff-Zieschang, N.; Xu, W.; Jiang, J.; Caruso, F. Coatings super-repellent to ultralow surface tension liquids. *Nat. Mater.* **2018**, *17*, 1040–1047.

(7) Peng, C.; Chen, Z.; Tiwari, M. K. All-organic superhydrophobic coatings with mechanochemical robustness and liquid impalement resistance. *Nat. Mater.* **2018**, *17*, 355–360.

(8) Liu, T. L.; Kim, C.-J. C. Turning a surface superrepellent even to completely wetting liquids. *Science* **2014**, *346*, 1096–1100.

(9) Lu, Y.; Sathasivam, S.; Song, J.; Crick, C. R.; Carmalt, C. J.; Parkin, I. P. Robust self-cleaning surfaces that function when exposed to either air or oil. *Science* **2015**, *347*, 1132–1135.

(10) Tuteja, A.; Choi, W.; Ma, M.; Mabry, J. M.; Mazzella, S. A.; Rutledge, G. C.; McKinley, G. H.; Cohen, R. E. Designing superoleophobic surfaces. *Science* **2007**, *318*, 1618–1622.

(11) Theato, P.; Sumerlin, B. S.; O'Reilly, R. K.; Epps III, T. H. Stimuli responsive materials. *Chem. Soc. Rev.* **2013**, *42*, 7055–7056.

(12) Shafranek, R. T.; Millik, S. C.; Smith, P. T.; Lee, C.-U.; Boydston, A. J.; Nelson, A. Stimuli-responsive materials in additive manufacturing. *Prog. Polym. Sci.* **2019**, *93*, 36–67.

(13) Huang, F.; Zhang, X.; Tang, B. Z.; Stimuli-responsive materials: A web themed collection. *Mater. Chem. Front.* **2019**, *3*, 10–11.

(14) Sun, H.; Kabb, C. P.; Sims, M. B.; Sumerlin, B. S. Architecture-transformable polymers: Reshaping the future of stimuli-responsive polymers. *Prog. Polym. Sci.* **2019**, *89*, 61–75.

(15) Rastogi, P.; Kandasubramanian, B. Breakthrough in the printing tactics for stimuli-responsive materials: 4D printing. *Chem. Eng. J.* **2019**, *366*, 264–304.

(16) Pan, S.; Guo, R.; Bertleff-Zieschang, N.; Li, S.; Besford, Q. A.; Zhong, Q.-Z.; Yun, G.; Zhang, Y.; Cavalieri, F.; Ju, Y.; Goudeli, E.; Richardson, J. J.; Caruso, F. Modular assembly of host–guest metal–phenolic networks using macrocyclic building blocks. *Angew. Chem. Int. Ed.* **2020**, *59*, 275–280.

(17) Wang, Y.; Gong, X. Special oleophobic and hydrophilic surfaces: Approaches, mechanisms, and applications. *J. Mater. Chem. A* **2017**, *5*, 3759–3773.

(18) Hou, X.; Zhang, Y. S.; Santiago, G. T.-d.; Alvarez, M. M.; Ribas, J.; Jonas, S. J.; Weiss, P. S.; Andrews, A. M.; Aizenberg, J.; Khademhosseini, A. Interplay between materials and microfluidics. *Nat. Rev. Mater.* **2017**, *2*, 17016.

(19) Kreder, M. J.; Alvarenga, J.; Kim, P.; Aizenberg, J. Design of anti-icing surfaces: Smooth, textured or slippery? *Nat. Rev. Mater.* **2016**, *1*, 15003.

(20) Liu, M.; Wang, S.; Jiang, L. Nature-inspired superwettability systems. *Nat. Rev. Mater.* ***2017***, *2*, 17036.

(21) Howarter, J. A.; Youngblood, J. P. Self-cleaning and anti-fog surfaces via stimuli-responsive polymer brushes. *Adv. Mater.* **2007**, *19*, 3838–3843.

(22) Singh, A. K.; Singh, J. K. Fabrication of zirconia based durable superhydrophobic–superoleophilic fabrics using non fluorinated materials for oil–water separation and water purification. *RSC Adv.* **2016**, *6*, 103632–103640.

(23) Movafaghi, S.; Wang, W.; Metzger, A.; Williams, D. D.; Williams, J. D.; Kota, A. K. Tunable superomniphobic surfaces for sorting droplets by surface tension. *Lab Chip* **2016**, *16*, 3204–3209.

(24) Brown, P. S.; Bhushan, B. Durable superoleophobic polypropylene surfaces. *Philos. Trans. R. Soc., A* **2016**, *374*, 20160193.

(25) Brown, P. S.; Bhushan, B. Liquid-impregnated porous polypropylene surfaces for liquid repellency. *J. Colloid Interface Sci.* **2017**, *487*, 437–443.

(26) Martin, S.; Bhushan, B. Transparent, wear-resistant, superhydrophobic and superoleophobic poly(dimethylsiloxane) (PDMS) surfaces. *J. Colloid Interface Sci.* **2017**, *488*, 118–126.

(27) O'Loughlin, T. E.; Martens, S.; Ren, S. R.; McKay, P.; Banerjee, S. Orthogonal wettability of hierarchically textured metal meshes as a means of separating water/oil emulsions. *Adv. Eng. Mater.* **2017**, *19*, 1600808.

(28) Demir, T.; Wei, L.; Nitta, N.; Yushin, G.; Brown, P. J.; Luzinov, I. Toward a long-chain perfluoroalkyl replacement: Water and oil repellency of polyethylene terephthalate (PET) films modified with perfluoropolyether-based polyesters. *ACS Appl. Mater. Interfaces* **2017**, *9*, 24318–24330.

(29) Singh, N.; Kakiuchida, H.; Sato, T.; Hönes, R.; Yagihashi, M.; Urata, C.; Hozumi, A. Omniphobic metal surfaces with low contact angle hysteresis and tilt angles. *Langmuir* **2018**, *34*, 11405–11413.

(30) Eom, S.; Kang, D. W.; Kang, M.; Choe, J. H.; Kim, H.; Kim, D. W.; Hong, C. S. Fine-tuning of wettability in a single metal-organic framework via postcoordination modification and its reduced graphene oxide aerogel for oil-water separation. *Chem. Sci.* **2019**, *10*, 2663–2669.

(31) Ursino, C.; Di Nicolò, E.; Gabriele, B.; Criscuoli, A.; Figoli, A. Development of a novel perfluoropolyether (PFPE) hydrophobic/hydrophilic coated membranes for water treatment. *J. Membr. Sci.* **2019**, *581*, 58–71.

(32) Jiang, P.; Zhang, L.; Guo, H.; Chen, C.; Wu, C.; Zhang, S.; Wang, Z. L. Signal output of triboelectric nanogenerator at oil–water–solid multiphase interfaces and its application for dual-signal chemical sensing. *Adv. Mater.* **2019**, *31*, e1902793.

(33) Deng, X.; Mammen, L.; Butt, H.-J.; Vollmer, D. Candle soot as a template for a transparent robust superamphiphobic coating. *Science* **2011**, *335*, 67–70.

(34) Li, Y.; Quere, D.; Lv, C.; Zheng, Q. Monostable superrepellent materials. *Proc. Nat. Acad. Sci. U.S.A.* **2017**, *114*, 3387–3392.

(35) Grigoryev, A.; Tokarev, I.; Kornev, K. G.; Luzinov, I.; Minko, S. Superomniphobic magnetic microtextures with remote wetting control. *J. Am. Chem. Soc.* **2012**, *134*, 12916–12919.

(36) Ichimura, K.; Oh, S.-K.; Nakagawa, M. Light-driven motion of liquids on a photoresponsive surface. *Science* **2000**, *288*, 1624–1626.

(37) Li, Z.; Cao, M.; Li, P.; Zhao, Y.; Bai, H.; Wu, Y.; Jiang, L. Surface-embedding of functional micro-/nanoparticles for achieving versatile superhydrophobic interfaces. *Matter* **2019**, *1*, 661–673.

(38) Wagner, N.; Kessler, D.; Theato, P. Reactive coatings in glass capillaries: Preparation of temperature- and light-responsive surfaces and accurate determination of wettability switching. *Macromol. Chem. Phys.* **2016**, *217*, 92–100.

(39) Pirani, F.; Angelini, A.; Ricciardi, S.; Frascella, F.; Descrovi, E. Laser-induced anisotropic wettability on azopolymeric micro-structures. *Appl. Phys. Lett.* **2017**, *110*, 101603.

(40) Kwon, G.; Panchanathan, D.; Mahmoudi, S. R.; Gondal, M. A.; McKinley, G. H.; Varanasi, K. K. Visible light guided manipulation of liquid wettability on photoresponsive surfaces. *Nat. Commun.* **2017**, *8*, 14968.

(41) Singh, V.; Huang, C.-J.; Sheng, Y.-J.; Tsao, H.-K. Smart zwitterionic sulfobetaine silane surfaces with switchable wettability for aqueous/nonaqueous drops. *J. Mater. Chem. A* **2018**, *6*, 2279–2288.

(42) Barman, J.; Shao, W.; Tang, B.; Yuan, D.; Groenewold, J.; Zhou, G. Wettability manipulation by interface-localized liquid dielectrophoresis: Fundamentals and applications. *Micromachines* **2019**, *10*, 329.

(43) Guselnikova, O.; Elashnikov, R.; Postnikov, P.; Svorcik, V.; Lyutakov, O. Smart, piezo-responsive polyvinylidenefluoride/polymethylmethacrylate surface with triggerable water/oil wettability and adhesion. *ACS Appl. Mater. Interfaces* **2018**, *10*, 37461–37469.

(44) Kota, A. K.; Kwon, G.; Choi, W.; Mabry, J. M.; Tuteja, A. Hygro-responsive membranes for effective oil–water separation. *Nat. Commun.* **2012**, *3*, 1025.

(45) Brown, P. S.; Bhushan, B. Bioinspired, roughness-induced, water and oil super-philic and super-phobic coatings prepared by adaptable layer-by-layer technique. *Sci. Rep.* **2015**, *5*, 14030.

(46) Pan, S.; Guo, R.; Xu, W. Durable superoleophobic fabric surfaces with counterintuitive superwettability for polar solvents. *AIChE J.* **2014**, *60*, 2752–2756.

(47) Darmanin, T.; Guittard, F. Highly polar linkers (urea, carbamate, thiocarbamate) for superoleophobic/superhydrophobic or oleophobic/hydrophilic properties. *Adv. Mater. Interfaces* **2015**, *2*, 1500081.

(48) Durán, I. R.; Laroche, G. Current trends, challenges, and perspectives of anti-fogging technology: Surface and material design, fabrication strategies, and beyond. *Prog. Mater. Sci.* **2019**, *99*, 106–186.

(49) Butt, H.-J.; Berger, R.; Steffen, W.; Vollmer, D.; Weber, S. A. L. Adaptive wetting—Adaptation in wetting. *Langmuir* **2018**, *34*, 11292−11304.

(50) Tang, S.; Bhimavarapu, Y.; Gulec, S.; Das, R.; Liu, J.; N'guessan, H.; Whitehead, T.; Yao, C.-W.; Tadmor, R. Droplets sliding down a vertical surface under increasing horizontal forces. *Langmuir* **2019**, *35*, 8191−8198.

(51) Yadav, S.; Gulec, S.; Tadmor, R.; Lian, I. A novel technique enables quantifying the molecular interaction of solvents with biological tissues. *Sci. Rep.* **2019**, *9*, 9319.

(52) Maier, G. P.; Rapp, M. V.; Waite, J. H.; Israelachvili, J. N.; Butler, A. Adaptive synergy between catechol and lysine promotes wet adhesion by surface salt displacement. *Science* **2015**, *349*, 628–632.

(53) Park, J.; Urata, C.; Masheder, B.; Cheng, D. F.; Hozumi, A. Long perfluoroalkyl chains are not required for dynamically oleophobic surfaces. *Green Chem.* **2013**, *15*, 100−104.

(54) Yang, J.; Zhang, Z.; Xu, X.; Zhu, X.; Men, X.; Zhou, X. Superhydrophilic–superoleophobic coatings. *J. Mater. Chem.* **2012**, *22*, 2834–2837.

(55) Jiang, J.; Zhang, G.; Wang, Q.; Zhang, Q.; Zhan, X.; Chen, F. Novel fluorinated polymers containing short perfluorobutyl side chains and their super wetting performance on diverse substrates. *ACS Appl. Mater. Interfaces* **2016**, *8*, 10513−10523.

(56) Guerra, P.; Kim, M.; Kinsman, L.; Ng, T.; Alaee, M.; Smyth, S. A. Parameters affecting the formation of perfluoroalkyl acids during wastewater treatment. *J. Hazard. Mater.* **2014**, *272*, 148–154.

(57) Darmanin, T.; Guittard, F. Molecular design of conductive polymers to modulate superoleophobic properties. *J. Am. Chem. Soc.* **2009**, *131*, 7928–7933.

(58) Davis, A.; Yeong, Y. H.; Steele, A.; Loth, E.; Bayer, I. S. Spray impact resistance of a superhydrophobic nanocomposite coating. *AIChE J.* **2014**, *60*, 3025–3032.

(59) Filippidi, E.; Cristiani, T. R.; Eisenbach, C. D.; Waite, J. H.; Israelachvili, J. N.; Ahn, B. K.; Valentine, M. T. Toughening elastomers using mussel-inspired iron-catechol complexes. *Science* **2017**, *358*, 502–505.

(60) Ejima, H.; Richardson, J. J.; Liang, K.; Best, J. P.; Van Koeverden, M. P.; Such, G. K.; Cui, J.; Caruso, F. One-step assembly of coordination complexes for versatile film and particle engineering. *Science* **2013**, *341*, 154–157.

(61) Gu, Y.; Alt, E. A.; Wang, H.; Li, X.; Willard, A. P.; Johnson, J. A. Photoswitching topology in polymer networks with metal–organic cages as crosslinks. *Nature* **2018**, *560*, 65–69.

(62) Zhu, Z.; Tian, Y.; Chen, Y.; Gu, Z.; Wang, S.; Jiang, L. Superamphiphilic silicon wafer surfaces and applications for uniform polymer film fabrication. *Angew. Chem. Int. Ed.* **2017**, *56*, 5720–5724.

(63) Jia, X.; Minami, K.; Uto, K.; Chang, A. C.; Hill, J. P.; Nakanishi, J.; Ariga, K. Adaptive liquid interfacially assembled protein nanosheets for guiding mesenchymal stem cell fate. *Adv. Mater.* **2020**, *32*, 1905942.

(64) Boyken, S. E.; Benhaim, M. A.; Busch, F.; Jia, M.; Bick, M. J.; Choi, H.; Klima, J. C.; Chen, Z.; Walkey, C.; Mileant, A.; Sahasrabuddhe, A.; Wei, K. Y.; Hodge, E. A.; Byron, S.; Quijano-Rubio, A.; Sankaran, B.; King, N. P.; Lippincott-Schwartz, J.; Wysocki, V. H.; Lee, K. K.; Baker, D. De novo design of tunable, pH-driven conformational changes. *Science* **2019**, *364*, 658–664.

(65) Guo, J.; Ping, Y.; Ejima, H.; Alt, K.; Meissner, M.; Richardson, J. J.; Yan, Y.; Peter, K.; von Elverfeldt, D.; Hagemeyer, C. E.; Caruso, F. Engineering multifunctional capsules through the

assembly of metal–phenolic networks. *Angew. Chem. Int. Ed.* **2014**, *53*, 5546–5551.

(66) Martell, A. E.; Smith, R. M. *Critical Stability Constants*. *Volume 5. First Supplement*, Springer Science+Business Media, New York, **1982**, 340–355.

(67) Tadmor, R.; Das, R.; Gulec, S.; Liu, J.; N'guessan, H. E.; Shah, M.; Wasnik, P. S.; Yadav, S. B. Solid–liquid work of adhesion. *Langmuir* **2017**, *33*, 3594−3600.

(68) Tadmor, R. Line energy and the relation between advancing, receding, and Young contact angles. *Langmuir* **2004**, *20*, 7659−7664.

(69) Fumagalli, L.; Esfandiar, A.; Fabregas, R.; Hu, S.; Ares, P.; Janardanan, A.; Yang, Q.; Radha, B.; Taniguchi, T.; Watanabe, K.; Gomila, G.; Novoselov, K. S.; Geim, A. K. Anomalously low dielectric constant of confined water. *Science* **2018**, *360*, 1339–1342.

(70) Computational Chemistry Comparison and Benchmark Database, Release 20 (August **2019**), Standard Reference Database 101, National Institute of Standards and Technology. *Electric Dipole Moments Calculated from Atom Charges Compared to Dipoles from the Wavefunction*. https://cccbdb.nist.gov/diprecalcx.asp. (accessed 18 December 2019)

(71) Wohlfarth, C. *Static Dielectric Constants of Pure Liquids and Binary Liquid Mixtures. Landolt-Börnstein – Group IV Physical Chemistry, Volume 6*, Springer-Verlag Berlin and Heidelberg GmbH & Co. KG, **1991**, 11−213.

(72) Snyder, L. R. Classification of the solvent properties of common liquids. *J. Chromatogr.* **1978**, *92*, 223–234.

(73) Reichardt, C. *Solvents and Solvent Effects in Organic Chemistry*, Third Updated and Enlarged Edition, WILEY-VCH Verlag GmbH & Co. KGaA, Weinheim, **2003**, 418–424.

(74) Guo, J.; Richardson, J. J.; Besford, Q. A.; Christofferson, A. J.; Dai, Y.; Ong, C. W.; Tardy, B. L.; Liang, K.; Choi, G. H.; Cui, J.; Yoo, P. J.; Yarovsky, I.; Caruso, F. Influence of ionic strength on the deposition of metal–phenolic networks. *Langmuir* **2017**, *33*, 10616–10622.

(75) Virga, E.; Spruijt, E.; de Vos, W. M.; Biesheuvel, P. M. Wettability of amphoteric surfaces: The effect of pH and ionic strength on surface ionization and wetting. *Langmuir* **2018**, *34*, 15174–15180.

(76) Pan, S.; Goudeli, E.; Chen, J.; Lin, Z.; Zhong, Q.-Z.; Zhang, W.; Yu, H.; Guo, R.; Richardson, J. J.; Caruso F. Exploiting supramolecular dynamics in metal–phenolic networks to generate metal–oxide and metal–carbon networks. *Angew. Chem. Int. Ed.* **2021**, DOI: 10.1002/anie.202103044.

(77) Tadmor, R.; Bahadur, P.; Leh, A.; N'guessan, H. E.; Jaini, R.; Dang, L. Measurement of lateral adhesion forces at the interface between a liquid drop and a substrate. *Phys. Rev. Lett.* **2009**, *103*, 266101.

Table of Contents (TOC) graphic entry